

Dispersive photoconductivity in the layered perovskite $\text{Nd}_2\text{Ti}_3\text{O}_9$

Bertrand Dulieu, Jacques Bullo, and Jany Wéry

Laboratoire de Physique Cristalline, Institut des Matériaux de Nantes, 2 rue de la Houssinière, 44072 Nantes Cedex 03, France

Mireille Richard and Luc Brohan

Laboratoire de Chimie des Solides, Institut des Matériaux de Nantes, 2 rue de la Houssinière, 44072 Nantes Cedex 03, France

(Received 31 May 1995; revised manuscript received 29 November 1995)

We report on relaxation of trapped photocarriers in the layered perovskite $\text{Nd}_2\text{Ti}_3\text{O}_9$, which contains a high density of oxygen vacancies. It is shown that after termination of cw illumination a nonexponential relaxation of photo-created carriers with an increasingly slow rate of decay is observed. This phenomenon, also named persistent photoconductivity, only occurs when light is absorbed at the sample surface and under vacuum; in the presence of air a very fast return to equilibrium is observed. Typical photocurrent (i_p) decays recorded after visible or uv excitation and their variations with temperature are reported. In all cases we found that the instantaneous lifetime follows a power-law time dependence: $\tau_{\text{inst}} = i_p(t)/|di_p/dt| \propto t^\alpha$ ($0 < \alpha < 1$), indicative of dispersive behavior. Photocurrent decays could be fitted with great accuracy, for times up to 24 h, to a stretched exponential relaxation law: $i_p(t) = i_p(0)\exp[-(t/\tau)^\beta]$, with $\beta = 1 - \alpha$. On this basis it is assumed that randomly distributed oxygen vacancies acting as trapping centers for electrons are submitted to dispersive diffusion, which thus controls carrier recombination. The distribution of localized states in the gap is discussed in terms of a random distribution of oxygen vacancies. An Urbach-type edge between 2.20 and 2.75 eV below E_c is revealed by the photocurrent excitation spectrum, whereas an exponential distribution of trapping centers close to E_c of width ~ 60 meV is deduced from the temperature dependence of β . The observed complex variations of the relaxation time τ with temperature and pressure are linked to the presence of chemisorbed species in oxygen vacancies and rationalized in terms of oxygen coverage of the sample surface.

I. INTRODUCTION

For several years titanates adopting the perovskite structure have attracted interest as materials for applications in the fields of catalysis and dielectric properties. In this structure, the $B\text{-X}_6$ octahedra share corners in the three crystallographic directions; B is a metal and X is an oxygen or halogen atom [see Fig. 1(a)]. The layered perovskites $A_2\text{Nd}_2\text{Ti}_3\text{O}_{10}$ ($A = \text{K}$ or Na) are based upon this structural feature. The same holds for the compound under study, $\text{Nd}_2\text{Ti}_3\text{O}_9$ (NTO), which is obtained from $\text{K}_2\text{Nd}_2\text{Ti}_3\text{O}_{10}$ by acid exchange followed by heating at 873 K. In Fig. 1(b) and Fig. 1(c) are shown the structures of the titanates we are interested in and their relationship to the perovskite structure. The layers are constituted of three perovskite slabs and are stacked one upon the other with a $1/2$ gliding along two directions. It should be noted that in $A_2\text{Nd}_2\text{Ti}_3\text{O}_{10}$ ($A = \text{K}$ or Na) the alkali metal occupies the interlayer site whereas the rare earth is situated in the 12-fold coordinated intralayer position. $\text{Nd}_2\text{Ti}_3\text{O}_9$ has a similar structure but contains a high density of oxygen vacancies as compared to $\text{K}_2\text{Nd}_2\text{Ti}_3\text{O}_{10}$. These vacancies are distributed on anionic sites pointing towards the interlayer space. In addition, one-third of the intralayer neodymium cations migrate to occupy positions corresponding to two-thirds of the oxygen vacancies. In a rather rough description one can consider that one-half of the two oxygen atoms of $A_2\text{Nd}_2\text{Ti}_3\text{O}_{10}$ occupying all anionic sites pointing towards the interlayer space have been replaced by $2/3 \text{Nd}^{3+}$ and $1/2 \text{O}^{2-}$ vacancies statistically distributed. Details on the structural characterization of these materials were recently reported.^{1,2}

Some layered perovskites have revealed interesting catalytic or photocatalytic properties. This is the case of niobates $AA'_2\text{Nb}_3\text{O}_{10}$, with $A =$ alkali metal and $A' = \text{Ca}$ or Pb ,^{3,4} or other metal cations $\text{Bi}_2\text{O}_2(A_{n-1}B_n\text{O}_{3n+1})$, with $A = \text{Ba}$, Pb , or Sr and $B = \text{Ti}$, Nb , or Ta .⁵ Photoexcitation of powder-semiconductor-liquid systems has been extensively studied in recent years aiming in particular at water depollution.⁶ Photocatalytic tests performed upon NTO showed that this material has a weak activity as compared to the commonly used TiO_2 .^{7,8} The redox reactions involved in heterogeneous photocatalysis being quite dependent upon the surface properties of the powder photocatalyst, photoconductivity (PC) studies were undertaken in order to obtain information on

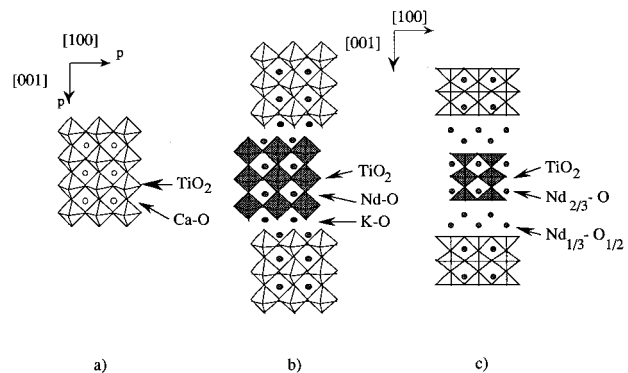


FIG. 1. (a) Perovskite structure, (b) structure of $\text{K}_2\text{Nd}_2\text{Ti}_3\text{O}_{10}$, and (c) structure of the oxygen-vacancy compound $\text{Nd}_2\text{Ti}_3\text{O}_9$.

electron-hole creation, charge trapping, and recombination at the surface, where the density of intrinsic defects due to oxygen vacancies is quite large.

The most prominent feature of PC in this material is the occurrence, after termination of illumination, of a nonexponential relaxation of photogenerated carriers with an increasingly slow rate of decay. This excess nonequilibrium conductance is often named “persistent photoconductivity” although dispersive photoconductivity seems more appropriate; it has been observed in various semiconductors like CdS:Ag:Cl,⁹ in the interface of $\text{Al}_x\text{Ga}_{1-x}\text{As-GaAs}$,¹⁰ and in the organic conducting polymer polyparaphenylenevinylene.¹¹ More generally, nonexponential relaxation has been observed in many physical systems such as, for example, dielectric relaxation in glassy media,¹² strain recovery in polymers,¹³ or relaxation in the electronic properties of amorphous hydrogenated silicon.¹⁴ Relaxation toward equilibrium in disordered media is often described by the so-called stretched exponential decay (Kolhrausch’s law):

$$\phi(t) = \phi(0) \exp\left(-\left(\frac{t}{\tau}\right)^\beta\right) \quad (1.1)$$

where $0 < \beta < 1$. Equation (1.1) was found to be quite general and was successfully applied to a variety of experimental data.¹⁵

In this paper we show that photocreated carriers in NTO decay with an instantaneous lifetime obeying a power-law time dependence and that their decay kinetics is accurately fitted to Eq. (1.1) for very long time periods at various temperatures. It is shown that these features are characteristic of photons absorbed at the sample surface. Assuming that carriers are trapped into oxygen vacancies, we established a model based on the dispersive diffusion of vacancies which leads to Eq. (1.1). The temperature dependence of the exponent β is reported and discussed together with the influence of chemisorbed oxygen on the variations of the relaxation time τ with temperature.

II. EXPERIMENT

The precursor of NTO, $\text{K}_2\text{Nd}_2\text{Ti}_3\text{O}_{10}$, was prepared by conventional solid state methods. Dry Nd_2O_3 (preheated at 1173 K), TiO_2 (anatase), and potassium nitrate in molar proportions 1:3:2.4 were ground and pressed to form a pellet and fired in a platinum crucible in air at 1273 K for 1 day. Acid exchange was achieved at room temperature in an aqueous solution. $\text{K}_2\text{Nd}_2\text{Ti}_3\text{O}_{10}$ was immersed in a 100-fold excess (by weight) of 1M HNO_3 for 4 days. The resulting product was retrieved by several cycles of centrifugation, and washed with distilled water and acetone before drying under vacuum. The oxygen-vacancy compound NTO was obtained by firing the exchanged phase at 873 K for 6 h.¹⁸ In order to test reproducibility two batches of NTO were separately synthesized, from which samples 1 and 2 were prepared.

Optical absorption spectra of NTO and $\text{K}_2\text{Nd}_2\text{Ti}_3\text{O}_{10}$ were measured by dispersing the powder materials into KBr to form pellets. For photoconductivity measurements powderlike NTO samples were pressed under about 50 bars for 2 min and then annealed in air at 873 K for 6 h to increase compactness. The obtained pellets are ~ 3 mm thick with

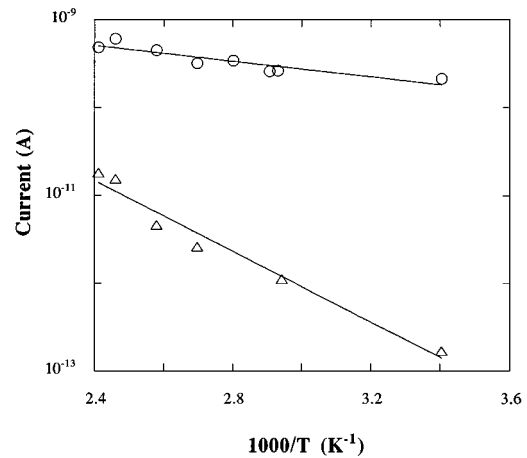


FIG. 2. Temperature dependence of the dark current (open triangles) and of the photocurrent (open circles) in sample 1 ($\lambda_{\text{exc}} = 457.9$ nm).

o.d. ~ 8 mm. Surface gold strips with a 2 mm interelectrode spacing were evaporated and contacted to the external circuit with an Ag-loaded epoxy resin. Ohmicity was checked up to a field of 10^3 V cm⁻¹. Measurements on sample 1 were made in a stainless cell which could be evacuated to a pressure of 5×10^{-6} mbar. In contrast, measurements on sample 2 were made in an Oxford cryostat which allowed a much lower pressure of $\sim 10^{-7}$ mbar to be reached.

Measurements of the PC decay kinetics were made under cw conditions using a Spectra Physics argon laser. Measurements on sample 1 were made by illuminating with the 457.9 nm line whereas those on sample 2 were made by illuminating with the mid-uv lines (333.6–363.8 nm), the light power falling on the interelectrode spacing (2×8 mm) being of the order of $6 \mu\text{W cm}^{-2}$. As shown below, under cw illumination, the photocurrent buildup does not reach steady state even after many hours (see Fig. 5) and as anticipated we found that the PC decay kinetics depends upon duration of the illumination period. In what follows the samples were irradiated for 3 h; at the end of this period the photocurrent to dark ratio is $\sim 10^4$ and the buildup rate has slowed down to $\sim 10^{-12}$ A min⁻¹. Photoexcitation spectra were recorded by illuminating with a constant monochromatic photon flux emerging from a xenon-lamp–monochromator setup, monitored by a Photodyne XLA radiometer. Standard electrometer, lock-in amplifier, and computer equipment were used for measuring the photocurrent. Before measurements the samples were heated at 453 K under vacuum for 12 h to remove adsorbed water.

III. RESULTS

A. Main features of photoconductivity

Under an electric field of 10^3 V cm⁻¹ at room temperature a dark current of $\sim 10^{-13}$ A was measured. In Fig. 2 is shown the temperature dependence of the dark current in the range 290–415 K; an activation energy of 0.40 eV was measured. The temperature dependence of the photocurrent i_p measured when illuminating at 457.9 nm is also shown in Fig. 2. i_p is thermally activated with an energy of 0.10 eV. The photon flux dependence of i_p ,

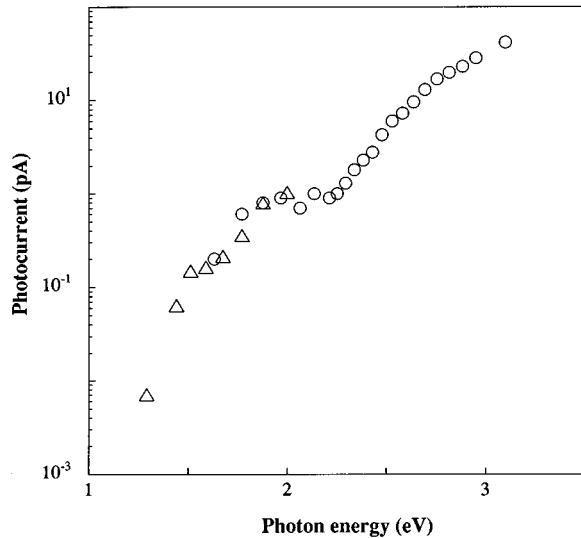


FIG. 3. Semilog plot of the photocurrent excitation spectrum at 300 K and at constant incident photon fluence. Open triangles: steady state measurements; open circles: measurements made after a fixed delay time of 10 min. Data are normalized at 1.88 eV.

$$i_p \propto \Phi^\gamma, \quad (3.1)$$

was measured at room temperature yielding $\gamma = 0.72$ at 457.9 nm. In Fig. 3 is shown a semilogarithmic plot of the photocurrent excitation spectra in NTO measured at constant incident flux. Some steady state measurements could be made in the energy range 1.25–2.10 eV. As discussed in Sec. III B, at energies higher than about 2.10 eV steady state is not reached after many hours and the photocurrent response could not be accurately measured. Therefore we recorded the photocurrent intensity at a fixed delay time after the beginning of illumination. As seen in Fig. 3 when normalized both sets of measurements are similar, showing that the photocurrent threshold is located at ~ 1.25 eV. It is interesting to compare the photoexcitation spectra with the absorption spectrum of the dispersed material into KBr pellets (Fig. 4). A wide absorption band extending from 200 to 380 nm, which may be attributed to the TiO_6 octahedra structure, is observed with an absorption edge which allows one to esti-

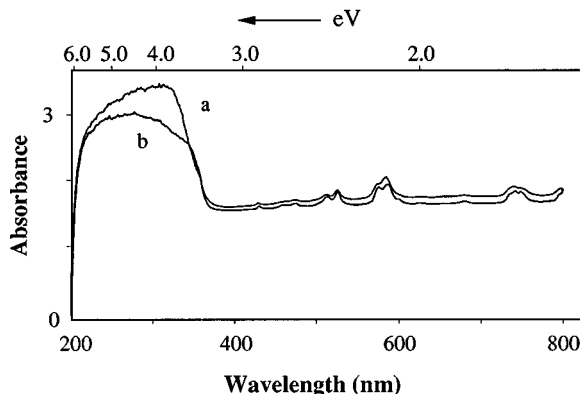


FIG. 4. Optical absorption spectra of NTO (curve *a*) and $\text{K}_2\text{Nd}_2\text{Ti}_3\text{O}_{10}$ (curve *b*) powders dispersed into KBr pellets.

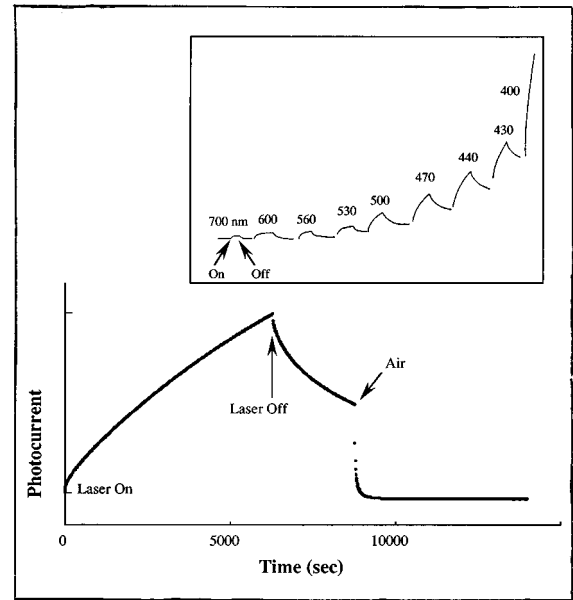


FIG. 5. Photocurrent buildup and decay in sample 2 under vacuum ($333.6 < \lambda_{\text{exc}} < 363.8$ nm). A very slow decay follows termination of illumination. If air is allowed to flow into the cell a quite fast decay and return to equilibrium are observed. Inset shows the wavelength dependence of the buildup and decay kinetics of photocarriers in NTO illuminated under vacuum for a period of 10 min. Steady state is reached within some minutes when $600 < \lambda_{\text{exc}} < 1000$ nm. At $\lambda_{\text{exc}} < 600$ nm the buildup and decay are increasingly longer.

mate an optical gap of the order of 3 eV, close to the energy gap of rutile, 3.01–3.05 eV.¹⁶ Between 400 and 800 nm several maxima are observed which are attributed to electronic transitions between the $4f$ orbitals of neodymium,¹⁷ yielding a flat spectrum up to at least 800 nm in contrast with the excitation spectrum.

B. Photocurrent decay

The main feature of PC is the very slow buildup and decay kinetics observed when illuminating with uv or visible light under vacuum. A typical example is shown in Fig. 5: a sluggish buildup is obtained under excitation with the mid-uv lines (333.6–363.8 nm) of an argon laser and steady state is not reached after many hours. When light is turned off an increasingly slower decay takes place. In contrast, we observed that PC decay kinetics depends upon the surface environment, as shown in Fig. 5. If during the slow decay *in vacuo*, air is allowed to flow into the cell, a very fast decay and return to equilibrium are obtained. The influence of the gas contacting the sample surface will be discussed in Sec. IV. All of the experiments to be described were carried out under vacuum. PC buildup and decay kinetics were found to depend not only upon temperature and light power as usual, but also upon the light wavelength. This is illustrated in the inset in Fig. 5. When illuminating at room temperature with the low power 1000–600 nm light emerging from a Xe-lamp–monochromator setup, steady state is reached within a few minutes. When the light wavelength is decreased the time required to reach steady state is increasingly longer and when illuminating with the high power Ar laser mid-uv lines,

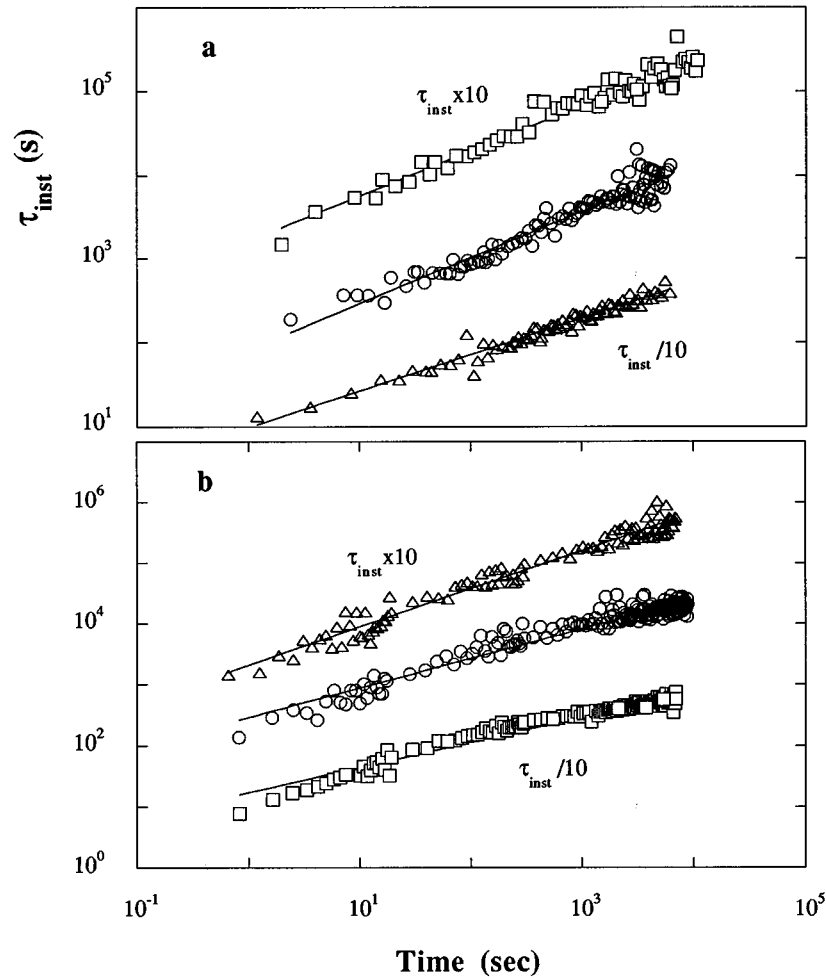


FIG. 6. Time dependence of the instantaneous lifetime $\tau_{\text{inst}} = i_p / |(di_p/dt)|$. Data were multiplied or divided by 10 as indicated for clarity. (a) Sample 1 ($\lambda_{\text{exc}} = 457.9$ nm). Open circles: 298 K, full laser power, $\alpha = 0.546$; open triangles: 393 K, full power, $\alpha = 0.433$; open squares: 298 K, at 0.25 power, $\alpha = 0.539$. (b) Sample 2 ($333.6 < \lambda_{\text{exc}} < 363.8$ nm). Open circles: 309 K, full laser power, $\alpha = 0.628$; open triangles: 368 K, full power, $\alpha = 0.482$; open squares: 298 K, at 0.25 power, $\alpha = 0.411$.

a very slow photoconductivity decay was observed for at least 24 h without return to thermal equilibrium. So it may be concluded that slow relaxation is observed at short wavelength, i.e., when light is absorbed at the sample surface.

Sheinkman *et al.*⁹ reviewed PC in inhomogeneous semiconductors and suggested a barrier model based upon the idea that the electric field due to inhomogeneities creates a recombination barrier which hinders recombination and a drift barrier which hinders current flow. The model predicts that the instantaneous lifetime defined by

$$\tau_{\text{inst}} = \frac{i_p(t)}{|di_p(t)/dt|} \quad (3.2)$$

is a linear function of time. We analyzed our data along these lines but found instead a power-law time dependence: $\tau_{\text{inst}} \propto t^\alpha$, $0 < \alpha < 1$, characteristic of dispersive behavior. Typical examples are shown in Fig. 6 for both samples. As seen, in spite of data scattering at long time due to inaccurate derivation, log-log plots of τ_{inst} as a function of time can be fitted with reasonable accuracy to a power law on a time period of the order of 2–3 h; at longer times the photocurrent decay is too slow to yield accurate data. This time dependence was

checked under different conditions by varying temperature between 298 and 450 K and light power in both samples.

The photocurrent decay can be fitted to the stretched exponential relaxation law [Eq. (1.1)] which applied to the photocurrent is written as:

$$i_p(t) = i_p(0) \exp\left(-\left(\frac{t}{\tau}\right)^\beta\right) \quad (3.3)$$

where τ is the relaxation time.

In Fig. 7 are shown typical log-log plots of the PC decay at various temperatures. In most cases the decay kinetics was measured on a time period of the order of 10^4 s. As seen, quite good fits were obtained. In one case the decay recording at 309 K was extended up to 24 h yielding a very good fit also (see inset in Fig. 7). In all cases we found that the relation $\alpha + \beta = 1$ is fairly well obeyed (see caption of Fig. 7). The temperature dependence of the exponent β , measured under constant light power, was studied in samples 1 and 2. In both specimens β depends linearly upon temperature, extrapolating close to 0 at 0 K: $\beta = T/T_0$ (Fig. 8), the slope yielding $T_0 = 720$ and 656 K for samples 1 and 2, respectively. We recall that sample 1 was illuminated at

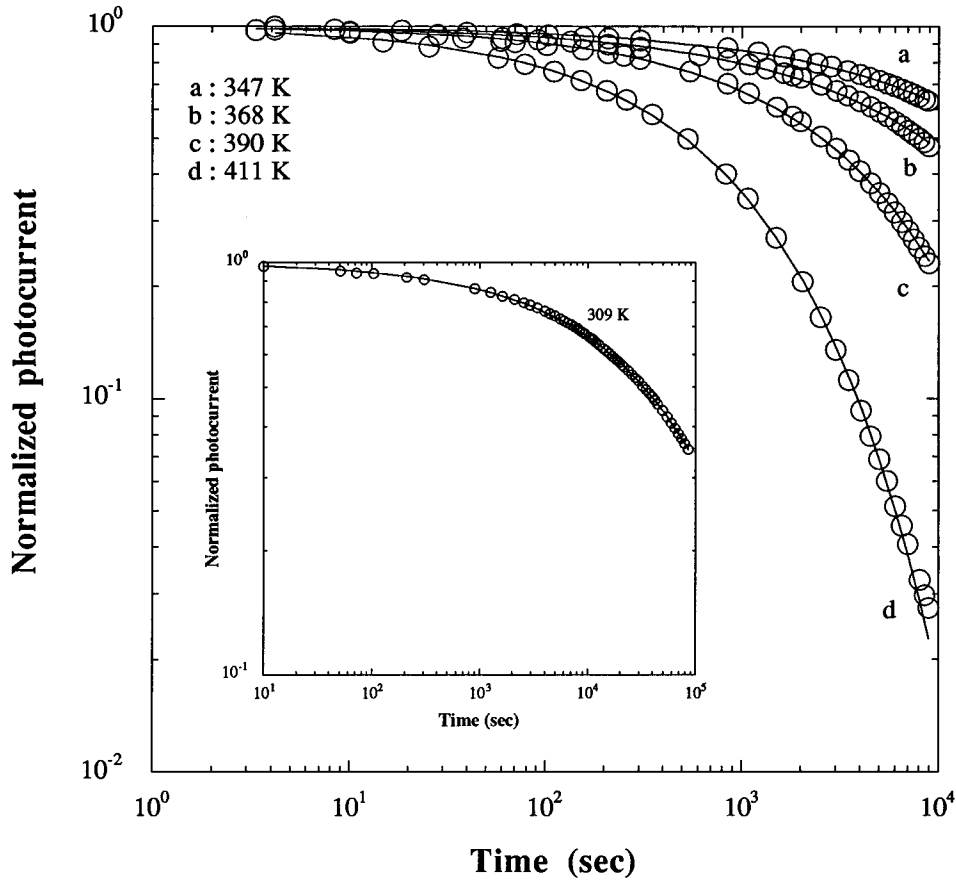


FIG. 7. Log-log plots of the normalized photocurrent decays at various temperatures in sample 2 ($333.6 < \lambda_{\text{exc}} < 363.8$ nm). The solid lines are the fits to Eq. (3.3), 95% of the data points being removed for clarity. The following β and τ values were extracted: $\beta = 0.529, 0.524, 0.587,$ and 0.598 ; $\tau = 41643, 16610, 4753,$ and 958 s at $T = 347, 368, 390,$ and 411 K, respectively. We find, respectively, $\alpha + \beta = 1.012, 1.006, 1.016,$ and 0.982 . Inset: decay kinetics of the normalized photocurrent measured at 309 K during 24 h ($333.6 < \lambda_{\text{exc}} < 363.8$ nm). The solid line is the fit to Eq. (3.3) and the open circles are experimental data, 95% of the data points being removed for clarity. $\beta = 0.431, \tau = 77656$ s, and $\alpha + \beta = 1.059$.

457.9 nm whereas sample 2 was illuminated in the mid-uv range (333.6–363.8 nm). As shown above (Fig. 5) the PC decay is profoundly affected when the photon energy is changed. Nevertheless, close values for T_0 are obtained, revealing a genuine material property. In Fig. 9 we present a semilogarithmic plot of the variations of the relaxation time τ as a function of reciprocal temperature. As seen, the variations are quite complex. Whereas an activated behavior is anticipated, we observed either small variations (sample 1) or the appearance of a pseudoplateau around room temperature (sample 2). This observation, which we relate to the presence of chemisorbed oxygen in oxygen vacancies, will be discussed in the next section.

IV. DISCUSSION

Analysis of PC and of its dispersive behavior in NTO may be summarized as follows.

- (i) The threshold for photocarrier generation is smaller than the band gap energy measured by optical absorption.
- (ii) The relaxation rate of photoexcited carriers depends upon the light penetration depth so that PC characterizes surface excitation.
- (iii) PC decay unambiguously follows the stretched exponential relaxation law for several hours.

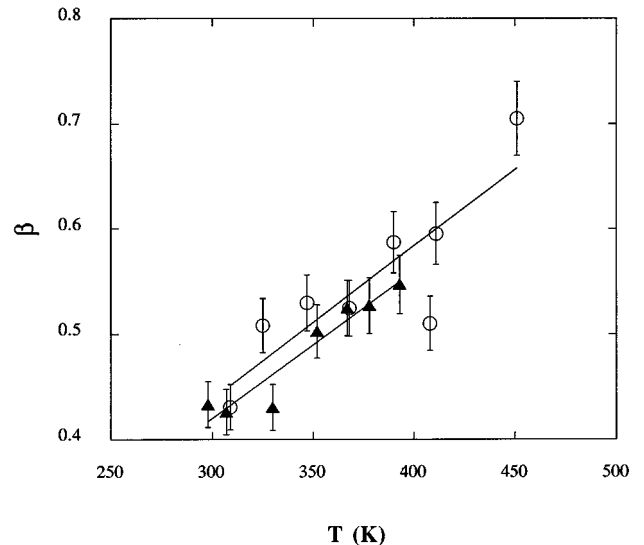


FIG. 8. Temperature dependence of the exponent β in Eq. (3.3): $\beta = T/T_0$. Closed triangles: sample 1, $T_0 = 720$ K; open circles: sample 2, $T_0 = 656$ K. The linear fits extrapolate at 0.0035 and 0.0018 at 0 K for specimens 1 and 2, respectively.

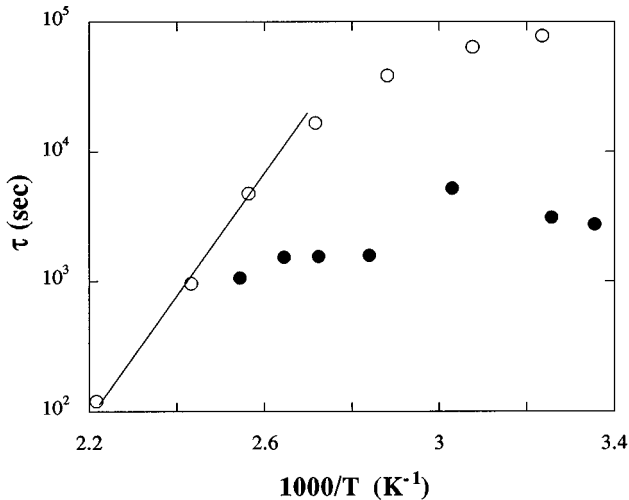


FIG. 9. Temperature dependence of the relaxation time τ . Solid circles: sample 1 (partial pressure 5×10^{-6} mbar); open circles: sample 2 (partial pressure $\sim 10^{-7}$ mbar). The difference between specimen 1 and specimen 2 is the ultimate vacuum which leads to a different coverage of the surface by chemisorbed oxygen atoms.

(iv) The exponent β depends linearly upon temperature.

(v) The complex variations of the relaxation time τ with temperature and pressure very likely may be related to chemisorbed oxygen atoms at the sample surface.

In order to introduce discussion several features deduced from structural studies should be taken into account. First, this material contains a high density of oxygen vacancies of about $5.6 \times 10^{-3} \text{ \AA}^{-3}$ corresponding to two vacancies per unit cell.⁸ It should be noted that this figure is purely indicative, because oxygen vacancies are not homogeneously distributed in the crystal volume but remain located in the interlayer space [see Fig. 1(c)]. Second, it has been shown^{1,8} that some disorder occurs during the acid exchange process, which is retained in NTO; but the basic layered crystal structure is preserved. Therefore amorphicity cannot account for the observed dispersive behavior of the instantaneous lifetime and of the stretched exponential relaxation law describing PC decay. We suggest instead that oxygen vacancies are randomly distributed at the surface of crystallites, giving rise to trapping centers in the gap.

Strong support to the existence of localized gap states comes from recent theoretical work on the influence of oxygen vacancies on the density of states (DOS) in TiO_2 .¹⁸⁻²⁰ These authors studied the effect of including 0%, 1%, 5%, and 10% oxygen vacancies at randomly selected sites. The authors found that a tail of donor states below the conduction band, extending a few tenths of an eV, grows with vacancy concentration in agreement with experimental reports.²¹ These states are localized and are playing the role of trapping centers. They examined both the bulk and the surface DOS and found the same results. In spite of the structural differences between rutile TiO_2 and the investigated layered perovskite, it may be expected that the gross features of the DOS upon incorporation of oxygen vacancies remain the same.

As shown above (Fig. 3) the threshold for photocarrier generation is about 1.75 eV smaller than the 3 eV band gap indicated by optical absorption data. This energy difference

suggests that there is a large DOS in the gap, the distribution of which is an important issue which has bearing on photocarrier transport. Information about the energy distribution of subgap states may be obtained by calculating the energy dependence of the absorption coefficient $\alpha(h\nu)$ from the photocurrent excitation spectrum $i_p(h\nu)$. This technique is widely used in the field of amorphous semiconductors, e.g., $\alpha\text{-Si:H}$.²²⁻²⁴ Indeed, the empirical photon flux dependence, Eq. (3.1), may be generalized to

$$i_p \propto (\alpha\Phi)^\gamma \quad (4.1)$$

so that experimental data are normalized as a function of photon energy:

$$\alpha(h\nu) = \alpha(h\nu_0) \frac{\Phi(h\nu_0)}{\Phi(h\nu)} \left[\frac{i_p(h\nu)}{i_p(h\nu_0)} \right]^{1/\gamma} \quad (4.2)$$

$h\nu_0$ is some reference energy where $\alpha(h\nu_0)$ is known from optical absorption measurements and $i_p(h\nu_0)$ is the corresponding photocurrent. It should be noted that accurate quantitative data are only obtained if several conditions are met,²³ in particular:

- (i) uniform electron-hole generation;
- (ii) only one type of carrier contributes to the photocurrent;
- (iii) the power-law dependence of i_p does not depend upon photon energy.

In the case at hand the photocurrent excitation spectrum was measured at constant incident photon fluence. As the exact value of $\alpha(h\nu_0)$ is unknown the ratio $\alpha(h\nu)/\alpha(h\nu_0)$ was calculated from Eq. (4.2). The semilogarithmic plot in Fig. 10 shows that between 2.20 and 2.75 eV $\alpha(h\nu)/\alpha(h\nu_0)$ exponentially decays over about two orders of magnitude, demonstrating the existence of an Urbach-type edge:

$$\alpha(h\nu) = \alpha_0 \exp\left(\frac{h\nu}{E_0}\right) \quad (4.3)$$

The slope allows measurement of a width ~ 120 meV. It should be emphasized that this value is indicative only, most of the conditions required to reach quantitative data remaining to be checked [except (iii)]. In addition, as stated in Sec. III A, $i_p(h\nu)$ was measured after a fixed delay time following illumination; consequently, when the photon energy is increased both the carrier density and the response/relaxation time increase. Therefore we simply conclude the existence of an apparently broad exponential absorption edge located deep in the gap, close to the valence band, whose origin might be the random energy distribution of oxygen vacancies at the crystallite surface. Clearly, accurate meaningful information would come if a NTO single crystal with well-defined and controlled surface was available. Unfortunately the growth of such crystals remains a nontrivial task.

We proceed by examining the lower energy region ($h\nu \lesssim 2.2$ eV) where a broad shoulder is observed. When the exponential absorption edge contribution is subtracted an absorption band extending from ~ 2.3 to 1.2 eV peaking at ~ 2 eV is seen, which is likely due to extrinsic absorption. Indeed, a peak at 1.98 eV has been found in the PC spectrum of a TiO_2 single crystal, which was attributed to iron

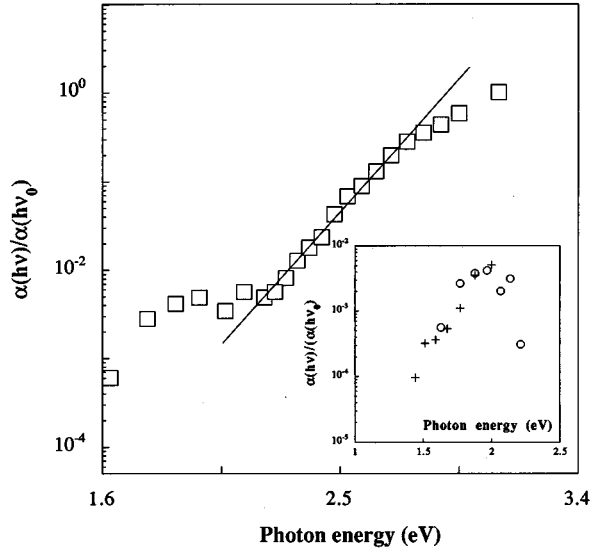


FIG. 10. Semilog plot of the ratio $\alpha(h\nu)/\alpha(h\nu_0)$ (open squares) calculated from Eq. (4.2) and the photocurrent excitation spectrum (open circles in Fig. 3) with $h\nu_0 = 3.1$ eV and $\gamma = 0.7$. The solid line is the fit to Eq. (4.3). Inset: open circles: absorption in the low energy region obtained by subtracting the contribution of the exponential absorption edge; crosses: low energy data obtained in steady state (Fig. 3).

impurity.²⁵ Introduction of such an impurity during synthesis of the NTO precursor (see Sec. II) is plausible. This peak would result from electron excitation from the Fe^{3+} level.

Insight into the qualitative picture of recombination in NTO may be gained from the observed temperature dependence of the relaxation time τ (Fig. 9). Indeed, we cannot ignore the influence of the ever-present residual gases O_2 , H_2O , and CO_2 in the measurement cell when working at a pressure of 5×10^{-6} mbar (sample 1) or $\sim 10^{-7}$ mbar (sample 2). τ should be strongly dependent upon the density of chemisorbed species in oxygen vacancies. This point is substantiated by the simple experiment described in Fig. 5: when air is introduced into the cell during the photocurrent decay the relaxation rate of photocarriers gets much faster. As oxygen coverage of the surface depends upon temperature and pressure, the variations of τ with temperature cannot follow the anticipated activated behavior:

$$\tau = \tau_0 \exp\left(\frac{E^*}{kT}\right) \quad (4.4)$$

which would characterize a “clean” surface, i.e., free of chemisorbed oxygen and other species. Working in UHV and at high temperature might perhaps allow one to obtain a “clean” surface. The trend in Fig. 9 agrees with such a statement. Whereas the temperature dependence of τ in sample 1, which was studied at 5×10^{-6} mbar, is not or weakly thermally activated, that of the sample 2, studied at $\sim 10^{-7}$ mbar, can be roughly fitted between 390 and 450 K to Eq. (4.4), yielding an apparent activation energy of 0.9 eV. We emphasize that this is a lower limit. Nevertheless, such a large value suggests that diffusion of oxygen vacancies is very likely the physical process underlying dispersive photoconductivity. This is why we put forward the simple

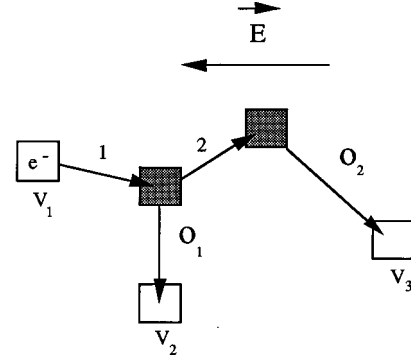


FIG. 11. Model of the relaxation of trapped electrons. An electron is trapped into the vacancy V_1 until a nearby oxygen O_1 diffuses into V_2 . The electron then makes a step into the newly formed vacancy, biased by the applied field \vec{E} . The pause and step process is repeated until recombination.

qualitative model depicted in Fig. 11. Oxygen vacancies are randomly distributed at the surface of the NTO crystallites and are submitted to a temperature-dependent diffusion mechanism. When light is applied electron-hole pairs are created and electrons get trapped into vacancies. A trapped electron pauses until a nearby vacancy is formed due to the jump of an oxygen atom. It then makes a step biased by the electric field. It thus moves by a succession of steps and pauses until recombination.

With this picture in hand and in order to reach a quantitative model, we start by briefly reviewing the basic features of charge transport in disordered media. It is characterized by two phenomena. The first one is dispersive transport observed in semiconductors like As_2Se_3 (Ref. 26) and amorphous hydrogenated silicon.²⁷ In these materials the drift mobility exhibits a power-law dependence, $\mu_D \propto t^{-\alpha}$, which was explained by Scher and Montroll²⁸ on the basis of the continuous time random walk model. The latter assumes that each carrier undergoes a random walk, composed of alternating steps and pauses, biased in the direction of the applied field with a pausing-time distribution $\Psi(t) \propto t^{-(1+\beta)}$, $\beta = 1 - \alpha$. Dispersion is due to the existence of an exponential energy distribution of traps below the conduction band edge: $\exp(-E/kT_0)$ where the width kT_0 is related to the dispersion parameter $1 - \alpha = T/T_0$. An alternative model proposed by Palmer, Stein, Abrahams, and Anderson,²⁹ who postulated a serial interpretation where the path to equilibrium involves many sequential correlated activation steps, leads to a time-dependent relaxation rate $k(t)$ in the rate equation

$$\frac{dn(t)}{dt} = -k(t)n(t) \quad (4.5)$$

where $n(t)$ is the density of photogenerated carriers.

The second characteristic of disordered media is the slow relaxation toward equilibrium described by a stretched exponential function [Eq. (1.1)]. Shlesinger and Montroll³⁰ studied this problem in the case of frozen dipoles in polymeric systems. They demonstrated that if the defects move in a continuous-time random walk and if the pausing-time distribution has a power-law time dependence, then relaxation has the form of a stretched exponential function. On this basis Kakalios *et al.*¹⁴ studied relaxation of the electronic proper-

ties of doped amorphous hydrogenated silicon and showed that dispersive diffusion of bonded hydrogen atoms induces relaxation of localized states, the functional form of which is well described by a stretched exponential law.

In the case at hand we assume that in NTO the jump of oxygen atoms into vacancies is submitted to a dispersive diffusion mechanism. Differences in the local environment generate a distribution of release times leading to a time-dependent diffusion coefficient

$$D_v = D_0(\omega t)^{-\alpha} \quad (4.6)$$

where ω is the attempt to hop frequency of oxygen atoms and D_0 is the temperature-dependent microscopic diffusion constant. In Eqs. (4.6) we use a formulation similar to that used and demonstrated by Kakalios¹⁴ in the case of the jump of hydrogen atoms in amorphous hydrogenated silicon. If in the rate equation (4.5) we write the time-dependent constant as

$$k(t) = \frac{D_0(\omega t)^{-\alpha}}{a^2}, \quad (4.7)$$

where we introduce the hopping distance a , it is seen that the instantaneous lifetime has a power-law time dependence:

$$\tau_{\text{inst}} = \frac{a^2 \omega^\alpha}{D_0} t^\alpha \quad (4.8)$$

as experimentally observed. Now integration of Eq. (4.5) using Eq. (4.7) immediately yields the stretched exponential functional form Eq. (1.1). So the stretched exponential relaxation law directly follows from the assumed dispersive diffusion of oxygen atoms.

We assumed above that the exponential absorption edge between 2.20 and 2.75 eV is due to the random distribution of oxygen vacancies. For the same reason we may assume that localized states below the conduction band edge are exponentially tailing. If so the continuous time random walk model¹⁵ predicts that the dispersion parameter increases linearly with temperature: $\beta = T/T_0$. Such a behavior is observed in Fig. 8 and we may conclude that trapping centers in NTO are exponentially distributed with a width $kT_0 \sim 60$ meV.

A last point remains to be discussed which concerns the complex variations of the relaxation time with temperature. Integration of the rate equation (4.5) with a time-dependent rate constant allows one to obtain

$$\tau = \frac{1}{\omega} \exp\left[\frac{kT_0}{kT} \ln \frac{a^2 \beta \omega}{D_0}\right], \quad (4.9)$$

which shows that τ is expected to be thermally activated with an activation energy

$$E_\tau = kT_0 \ln\left(\frac{a^2 \beta \omega}{D_0}\right) \quad (4.10)$$

in contrast with experimental observations (Fig. 9). As said before, we interpret these data as being the signature of chemisorbed oxygen at the sample surface. Therefore we

take into account the coverage θ of the surface by residual oxygen, which as qualitatively shown above is temperature and pressure dependent:

$$\theta(T, P) = \frac{N_{\text{occ}}}{N_{\text{tot}}} \quad (4.11)$$

where $0 < \theta < 1$, N_{occ} is the density per surface unit of vacancies containing chemisorbed species, and N_{tot} is the density per surface unit of vacancies for a ‘‘clean’’ surface, i.e., free of chemisorbed species. Under these conditions the rate constant is written as

$$k(t) = \theta \frac{D_0(\omega t)^{-\alpha}}{a^2}, \quad (4.12)$$

which after integration of Eq. (4.5) leads to a temperature- and pressure-dependent activation energy:

$$E_\tau(T, P) = kT_0 \ln\left(\frac{a^2 \beta \omega}{\theta D_0}\right). \quad (4.13)$$

Equation (4.13) shows that when T is decreased or P is increased, θ increases and E_τ decreases in qualitative agreement with experiment. It should be noted that preliminary results on the pressure dependence of PC relaxation bring support to the assumption made above: $k(t) \propto \theta$.³¹ Now, as in the case of TiO₂(110) for which it was shown that desorption of chemisorbed gases like O₂, CO₂, CO, and H₂ is thermally activated,³² we write

$$N_{\text{occ}} = N_0 \exp\left(\frac{E_{\text{des}}}{kT}\right) \quad (4.14)$$

and write the microscopic diffusion constant as

$$D_0 = D^* \exp\left(-\frac{E_D}{kT}\right). \quad (4.15)$$

Combining Eqs. (4.11), (4.14), and (4.15) we obtain

$$\theta D_0 = D^* \frac{N_0}{N_{\text{tot}}} \exp\left(\frac{E_{\text{des}} - E_D}{kT}\right), \quad (4.16)$$

a quantity which may be deduced from experimental data, namely, from the power-law fits (Fig. 6) of τ_{inst} which now reads

$$\tau_{\text{inst}} = \frac{a^2 \omega^\alpha}{\theta D_0} t^\alpha. \quad (4.17)$$

Taking $\omega = 10^{13} \text{ s}^{-1}$ and $a = 4 \text{ \AA}$, we obtained the results presented in Fig. 12 where $\log_{10} \theta D_0$ is plotted as a function of reciprocal temperature. In spite of data scattering it is seen that in agreement with Eq. (4.16) θD_0 follows a temperature-activated law with an activation energy of 0.59 eV for sample 1 (partial pressure 5×10^{-6} mbar) and 0.62 eV for sample 2 (partial pressure $\sim 10^{-7}$ mbar). So we find that the activation energy of desorption of chemisorbed oxygen is larger than the diffusion constant of oxygen vacancies. This result is in agreement with the measured desorption

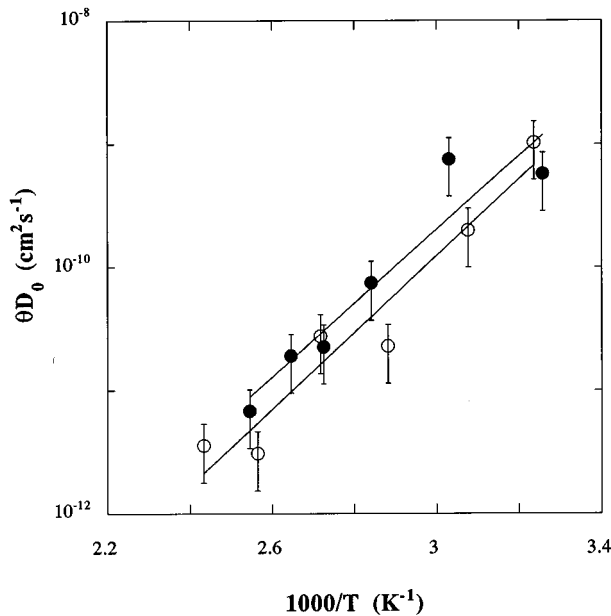


FIG. 12. Temperature dependence of the product θD_0 measured from the time dependence of τ_{inst} [Eq. (4.17)]. Solid circles: sample 1 (partial pressure 5×10^{-6} mbar); open circles: sample 2 (partial pressure $\sim 10^{-7}$ mbar).

activation energy $E_{\text{des}} = 94 \text{ kJ mol}^{-1}$ of oxygen chemisorbed on TiO_2 ,³² which was found to be larger than the diffusion constant $E_D = 60 \text{ kJ mol}^{-1}$ of oxygen vacancies in TiO_2 .³³ In Fig. 12 we note that the preexponential factor

$D^* N_0 / N_{\text{tot}}$ is about four times larger in sample 1 than in sample 2 showing that N_0 increases with the partial pressure in the measurement cell.

V. CONCLUSION

The layered perovskite $\text{Nd}_2\text{Ti}_3\text{O}_9$ is characterized by a large surface density of randomly distributed oxygen vacancies which govern charge carrier transport. Assuming that dispersive diffusion of vacancies triggers relaxation of localized states in the gap, we can explain the dispersive behavior of the photoconductivity instantaneous lifetime and the functional form of the slow decay of photogenerated carriers after termination of illumination. Analysis of the photoconductivity excitation spectrum reveals the existence of an Urbach edge close to the valence band and of an unidentified defect below midgap. The temperature dependence of the exponent β characterizing the stretched exponential decay of photocarriers shows that a band tail of localized states, acting as trapping centers, is exponentially distributed below the conduction band edge. In order to reach a more complete understanding of the dynamics of photocreated carriers in this material, transient photoconductivity measurements will be undertaken in the near future.

The relaxation time characterizing recombination of photocarriers is strongly dependent upon coverage of the surface by chemisorbed oxygen atoms. To give account of the gross features of its variation with temperature and residual pressure, we assumed that the time-dependent rate constant is proportional to the density of chemisorbed oxygen atoms moving into vacancies. Pressure-dependent studies which are expected to bring support to this assumption are under way.

- ¹M. Richard, L. Brohan, and M. Tournoux, *J. Solid State Chem.* **112**, 245 (1994).
- ²M. Richard, L. Brohan, A. M. Marie, C. Roucau, and M. Tournoux, *J. Solid State Chem.* (to be published).
- ³J. Barrault, C. Grosset, M. Dion, M. Ganne, and M. Tournoux, *Appl. Catal. A* **88**, 197 (1992).
- ⁴J. Yoshimura, Y. Ebina, J. Kondo, and A. Tanaka, *J. Phys. Chem.* **97**, 1970 (1993).
- ⁵J. Barrault, C. Grosset, M. Dion, M. Ganne, and M. Tournoux, *Catal. Lett.* **16**, 203 (1992).
- ⁶N. Serpone and E. Pelizzetti, *Photocatalysis. Fundamentals and Applications* (Wiley Interscience, New York, 1982).
- ⁷J. M. Hermann (unpublished).
- ⁸M. Richard, Ph.D. thèse de l'Université de Nantes, 1994.
- ⁹M. K. Sheinkman, I. V. Markevich, and V. A. Khvostov, *Sov. Phys. Semicond.* **5**, 1654 (1972); M. K. Sheinkman and A. Ya. Shik, *ibid.*, **10**, 128 (1976).
- ¹⁰H. J. Queisser, *Phys. Rev. Lett.* **54**, 234 (1985); in *Proceedings of the 17th International Conference on the Physics of Semiconductors*, edited by J. D. Chadi and W. A. Harrison (Springer, New York, 1985), p. 1303; H. J. Queisser and D. E. Theodorou, *Phys. Rev. B* **33**, 4027 (1986).
- ¹¹C. H. Lee, G. Yu, and A. J. Heeger, *Phys. Rev. B* **47**, 15 543 (1993).
- ¹²G. Williams and D. C. Watts, *Trans. Faraday Soc.* **66**, 80 (1970).
- ¹³D. G. Le Grand, W. V. Olszewski, and J. T. Bendler, *J. Polym. Sci.* **25**, 1149 (1987).
- ¹⁴J. Kakalios, R. A. Street, and W. B. Jackson, *Phys. Rev. Lett.* **59**, 1037 (1987); J. Kakalios, in *Hopping and Related Phenomena*, edited by H. Fritzsche and M. Pollak (World Scientific, Singapore, 1990), p. 441.
- ¹⁵H. Scher, M. F. Shlesinger, and J. T. Bender, *Phys. Today* **44** (1), 26 (1991).
- ¹⁶D. C. Cronemeyer, *Phys. Rev.* **87**, 876 (1952).
- ¹⁷P. Caro, *Structure Électronique des Éléments de Transition*, (Presses Universitaires de France, Paris, 1976).
- ¹⁸J. W. Halley, M. T. Michalewicz, and N. Tit, *Phys. Rev. B* **41**, 10 165 (1990).
- ¹⁹N. Tit, J. W. Halley, and M. T. Michalewicz, *Surf. Interface Anal.* **18**, 87 (1992).
- ²⁰N. Tit, J. W. Halley, M. T. Michalewicz, and H. Shore, *Appl. Surf. Sci.* **65-66**, 246 (1993).
- ²¹V. E. Heinrich, G. Dresselhaus, and H. J. Zeiger, *Phys. Rev. Lett.* **36**, 1335 (1976).
- ²²R. J. Loveland, W. E. Spear, and A. Al-Sharbaty, *J. Non Cryst. Solids* **13**, 55 (1973).
- ²³G. Modell, D. A. Anderson, and W. Paul, *Phys. Rev. B* **22**, 1918 (1980).
- ²⁴B. Abeles, C. R. Wronski, T. Tiedje, and G. D. Cody, *Solid State Commun.* **36**, 537 (1980).
- ²⁵T. Iida and H. Nozaki, *Bull. Chem. Soc. Jpn.* **42**, 929 (1969).
- ²⁶G. Pfister, *Phys. Rev. Lett.* **33**, 1474 (1974).
- ²⁷T. Tiedje, in *Hydrogenated Amorphous Silicon, Part C: Elec-*

- tronic and Transport Properties*, edited by J. Pankove, Semiconductors and Semimetals Vol. 21 (Academic Press, New York, 1984), p. 207.
- ²⁸H. Scher and E. W. Montroll, Phys. Rev. B **12**, 2455 (1975).
- ²⁹R. G. Palmer, D. L. Stein, E. Abrahams, and P. W. Anderson, Phys. Rev. Lett. **53**, 958 (1984).
- ³⁰M. F. Shlesinger and E. W. Montroll, Proc. Natl. Acad. Sci. U.S.A. **81**, 1280 (1984).
- ³¹B. Dulieu, J. Bullo, and J. Wéry (unpublished).
- ³²W. Göpel, G. Røcker, and R. Feierabend, Phys. Rev. B **28**, 3427 (1983).
- ³³R. Haul and G. Dümbgen, J. Phys. Chem. Solids **26**, 1 (1965).